Chemical Geology 495 (2018) 118–130

Contents lists available at ScienceDirect

Chemical Geology

journal homepage: www.elsevier.com/locate/chemgeo

Seasonal changes in sulfur biogeochemistry of a dilute, dimictic Arctic lake: Implications for paired sulfur isotope records from ancient oceans

Seth A. Young[a,*], Sarah B. Cadieux[b], Yongbo Peng[c], Jeffrey R. White[d,e], Lisa M. Pratt[e]

[a] Department of Earth, Ocean and Atmospheric Science, Florida State University, Tallahassee, FL 32306, United States of America
[b] Environmental Science Program, Sweet Briar College, Sweet Briar, VA 24595, United States of America
[c] Department of Geology and Geophysics, Louisiana State University, Baton Rouge, LA 70803, United States of America
[d] School of Public and Environmental Affairs, Indiana University, Bloomington, IN 47405, United States of America
[e] Department of Earth and Atmospheric Sciences, Indiana University, Bloomington, IN 47405, United States of America

ARTICLE INFO

Editor: Michael E. B.

Keywords:
Low-sulfate
Sulfur isotope
Arctic
Lakes
Seasonally ice-covered

ABSTRACT

Calibration of ancient marine sulfate levels has been done largely using experimental studies of the kinetic isotope effect associated with microbial sulfate reduction and work from modern ocean basins or high-sulfate lakes that are largely restricted and meromictic. The sulfur isotope record of sulfates and sulfides from sedimentary sequences have been used to reconstruct sulfate levels throughout the geologic record and indicate that sulfate concentrations were low relative to modern oceans (28 mM) for most of Earth's history. Despite the higher potential for modern low-sulfate systems to be a better analog for ancient oceans, there are few sulfur isotope studies that have been carried out in these environments. Here, we present $\delta^{34}S$ systematics of a modern low-sulfate (~330–600 μM) euxinic lake on the ice-free margin of southwestern Greenland. We find large isotope fractionations (> 20‰) between water column sulfate and sulfides, with this fractionation increasing from 23.9‰ during open-water conditions to 42.0‰ under annual ice-cover. While these large kinetic isotope effects associated with microbial sulfate reduction (ε_{SR}) are expressed in the water column of this lake, the underlying sedimentary sulfides preserve a notably smaller range of $\delta^{34}S$ values (13.0–26.6‰). Geochemical modeling of our data suggests that the $\delta^{34}S$ of water column sulfate and sulfides, along with sedimentary sulfides are primarily controlled by ε_{SR} and a reservoir effect established under strong thermal stratification during open-water conditions. Under ice-covered conditions ε_{SR} appears to be the dominant control on $\delta^{34}S$ values, and when combining both seasonal data sets ε_{SR} increases as a function of sulfate levels in the lake. Sulfur isotopic data presented here highlight the complexity of seasonal biogeochemical cycling of sulfur in low-sulfate systems, and how system openness affects $\delta^{34}S$ fractionations in modern euxinic depositional environments. Specifically, a reservoir effect is only documented in the water column $\delta^{34}S$ data under open-water conditions, however a reservoir effect is apparent from sedimentary sulfides under both ice-cover and open-water conditions due to time averaging pyrite $\delta^{34}S$ values. Our results add to the growing body of work on modern low-sulfate systems to help further constrain the use of ancient $\delta^{34}S$ records for paleoenvironmental reconstructions.

1. Introduction

Cycling of sulfur across physiochemical gradients is a critical adaptation that organisms have evolved to gain energy from a series of reduction-oxidation (redox) reactions as an alternative to aerobic respiration (Johnston, 2010). Microbes with sulfur-fueled metabolisms are important components of ecosystems within stratified water bodies and have been throughout much of Earth's history (e.g., Crowe et al., 2014a; Fike et al., 2006; Fry et al., 1991; Gomes and Hurtgen, 2013; Johnston, 2011; Leavitt et al., 2013; Lyons, 1997; Poulton et al., 2010). Most of the sulfur within marine or freshwater systems on early Earth were derived from the oxidative weathering of sedimentary sulfides delivered via rivers as the anion sulfate (SO_4^{2-}), although weathering of evaporites played an important role increasingly through the Phanerozoic (Halevy et al., 2012; Wortmann and Paytan, 2012). The sulfate supplied to aquatic environments can be converted to hydrogen sulfide (H_2S) via microbial sulfate reduction (MSR) within anoxic portions of the water column and/or below the sediment-water interface. Conversely, anoxygenic phototrophic sulfur bacteria (i.e., green and purple sulfur bacteria) and chemotrophic microbes oxidize sulfide and fix

* Corresponding author.
E-mail address: sayoung2@fsu.edu (S.A. Young).

https://doi.org/10.1016/j.chemgeo.2018.08.013
Received 11 February 2018; Received in revised form 20 June 2018; Accepted 13 August 2018
Available online 16 August 2018

carbon dioxide when sulfidic conditions develop in the photic zone (Overmann and Tilzer, 1989; Overmann et al., 1991; Fike et al., 2015). The anoxic portion of the biogeochemical S cycle within stratified waters is driven by reduction and oxidation based metabolisms. The biogeochemical C and S cycles are intrinsically linked through MSR, which couples the oxidation of organic matter to the production of sulfide (e.g., Berner, 2004 and references therein). Over the last 40 million years MSR has likely been the dominant pathway for organic matter remineralization in anoxic marine settings, due to high-sulfate content (~28 mM) of the oceans (e.g., Jørgensen, 1982; Wortmann and Paytan, 2012). However, methanogenesis and methanotrophy can play a larger role in organic matter remineralization in low-sulfate environments and these processes could impact the concentrations of atmospheric greenhouse gases dramatically (Pavlov et al., 2003; Reeburgh, 2007; Weber et al., 2016).

Sulfur isotopic compositions of dissolved ions in the water column, along with minerals and organic matter in the sediments are sensitive indicators of sulfur utilization by microbes in natural environments. Sulfide produced by MSR can be isotopically depleted in ^{34}S by up to 70‰ relative to starting sulfate in laboratory experiments (Harrison and Thode, 1958; Habicht and Canfield, 1996; Canfield et al., 2010; Sim et al., 2011a, 2011b). Within an environment, expression of the MSR kinetic isotope effect ($\varepsilon_{SR} = \delta^{34}S_{SO4} - \delta^{34}S_{H2S}$) can vary widely in magnitude and is dependent upon cellular physiology/biochemistry and environmental conditions that affect the rates of microbial sulfate reduction (Leavitt et al., 2013 and reference therein). Although organic matter (electron donor) is often a limiting reactant in MSR, dissolved oxygen content, sulfate concentrations (electron acceptor), temperature, and nutrients can also strongly affect the rates of MSR and the magnitude of S isotopic fractionations between reactants and products (Canfield, 2001; Habicht et al., 2002; Johnston, 2010, 2011; Leavitt et al., 2013). Sulfide produced in marine sediments today is predominantly cycled back to sulfate via a series of oxidation reactions, although if iron is available it can be buried as pyrite (Canfield et al., 1992; Bottrell and Newton, 2006). The oxidative portions of the sulfur cycle impart modest isotope effects from sulfur disproportionation (~20‰; Canfield and Thamdrup, 1994; Habicht et al., 1998) to small fractionations from sulfide oxidizing bacterium (≤5‰; Kaplan and Rittenberg, 1964; Fry et al., 1988; Zerkle et al., 2009). Rates of pyrite burial in sedimentary environments are largely dependent upon sulfate concentrations, extent of organic matter burial, water-column redox state, and Fe^{2+} availability (Berner, 1985). Ultimately the sedimentary sulfur isotope records are largely reflective of the balance between sulfur oxidation reactions and pyrite burial, and these records have been used to assess marine sulfate concentrations throughout Earth's history.

The isotopic difference between sulfur in sulfate and sulfides in sedimentary rocks ($\Delta^{34}S$ or $^{34}\varepsilon_{GEO} = \delta^{34}S_{sulfate} - \delta^{34}S_{pyr}$) has been used to reconstruct marine sulfate concentrations of ancient oceans, with dramatic implications for the evolution of biogeochemical cycling, climate, and redox throughout Earth history (Canfield, 1998; Habicht et al., 2002; Leavitt et al., 2013). While fluid inclusions provide estimates of sulfate concentrations in Neoproterozoic and Phanerozoic oceans, the sedimentary records of them are scant (Horita et al., 2002; Lowenstein et al., 2003, 2005; Brennan et al., 2013; Spear et al., 2014). Paired $\delta^{34}S$ analyses of sulfate evaporites and carbonate-associated sulfate (CAS) with sedimentary pyrite provide high temporal resolution records that are more easily dated and correlated than fluid inclusions. Small $\Delta^{34}S$ values in sedimentary rocks (Canfield, 1998) in association with large $\Delta^{33}S$ anomalies ($\Delta^{33}S > 0 \pm 0.2$‰; whereas $\Delta^{33}S_{sample} = \delta^{33}S_{sample} - 0.515 \times \delta^{34}S_{sample}$) due to photolytic reactions of sulfur aerosols in an anoxic early Earth atmosphere (Farquhar et al., 2000, 2001) are consistent with sulfate being in trace quantities (< 2.5 μM) in Archean oceans (Habicht et al., 2002; Crowe et al., 2014b). Marine sulfate likely rose as high as low millimolar concentrations (1–2% of modern values, 28 mM) approximately 2.3–2.4 billion years ago concurrent with the Great Oxidation Event (GOE). The GOE was marked by disappearance of large anomalous fractionations of $\Delta^{33}S$ from the sedimentary record (Bekker et al., 2004; Guo et al., 2009) and expanded range of $\delta^{34}S$ fractionations (Canfield, 2005) among other sedimentary indicators (i.e., Holland, 2006). Sulfate concentrations in the global oceans probably remained low, a few millimolar, until the Neoproterozoic (1050 to 540 million years ago), when sulfate levels may have cycled from ~10 mM to 1 mM during the course of multiple 'Snowball Earth' glaciations (Hurtgen et al., 2002, 2006; Kah et al., 2004). Although a recent study of Paleoproterozoic evaporites suggest that sulfate concentrations could have been as high as 10 mM at ~2.0 Ga, just after the GOE (Blattler et al., 2018). Frequent large $\delta^{34}S$ fractionations ($\Delta^{34}S > 50$‰) have been documented throughout the late Neoproterozoic and Phanerozoic sedimentary records and have been linked to increased sulfate concentrations and corresponding O_2 levels (Fike et al., 2006; Gill et al., 2007, 2011; Wortmann and Paytan, 2012). Sulfur isotope proxy records generally indicate that sulfate levels were variable and low relative to modern oceans (28 mM) throughout most of Earth history, with a general increase in concentration with each geologic era (Habicht et al., 2002; Kah et al., 2004; Holland, 2006; Gill et al., 2007).

The geologic record of marine sulfate inventory has been aligned largely using work from modern ocean basins or high-sulfate lakes that are mostly restricted and meromictic (e.g., Fry et al., 1991; Lyons, 1997; Lyons et al., 2003; Gilhooly et al., 2016). Although numerous sulfur isotope systematic studies of modern oceanic settings have been done (e.g., Chanton et al., 1987, 1991, 1993), there are few sulfur isotopic studies of modern low-sulfate systems, despite a greater potential to being more suitable analogs to Earth's ancient oceans (e.g., Crowe et al., 2014b; Gomes and Hurtgen, 2015). Recent work in low-sulfate lacustrine environments have shown that $\Delta^{34}S$ is controlled by both the fraction of the sulfate reservoir consumed during sulfate reduction and location of pyrite formation (reservoir effect), thus strongly influencing the $\delta^{34}S_{pyr}$ preserved in sediments (Hartmann and Nielsen, 1969, 2012). This study aims to add to the recent growing body of work in low sulfate systems that not only demonstrate the importance of the kinetic isotope effects associated with microbial sulfate reduction (ε_{SR}) but also the reservoir effect on $\delta^{34}S$ variations within these environments. Here, we report $\delta^{34}S$ values of water column profiles of sulfate, hydrogen sulfide, and sedimentary sulfide minerals near the sediment-water interface to assess seasonal variability in microbial sulfur cycling within a small Arctic lake in western Greenland. Our data show how the reservoir effect strongly influences $\delta^{34}S_{SO4}$ and $\delta^{34}S_{H2S}$ values that are recorded within open-water conditions while kinetic isotope effects become the dominate control on water-column microbial sulfur cycling under ice-covered conditions. To the best of our knowledge this study provides the first sulfur isotope systematics under both ice-covered and open-water conditions in a low-sulfate periglacial lacustrine system which significantly adds to our understanding of seasonal cycling of sulfur within low-sulfate aqueous environments. When our results are combined with other recent studies of low-sulfate systems they provide key constraints on paleoenvironmental interpretations of $\Delta^{34}S$ records from ancient marine sediments and evaluating the evolution of the marine reservoir of sulfate.

2. Background

The ice-free margin of Greenland exposes several deeply eroded Paleoproterozoic tectonic terranes separated by strongly deformed orogenic belts such as the bedrock in the Kangerlussuag region (Fig. 1A) which is part of the Nagssugtoqidian Orogeny (Henriksen et al., 2009). The Nagssugtoqidian folded belt is inferred to extend beneath the ice sheet to the Ammassalik region in South-East Greenland. Folding resulted from a collision between the North Atlantic Craton of southern Greenland and the Rinkian metamorphic terrane to the north. The Nagssugtoqidian belt is divided into three tectonic segments (van Gool

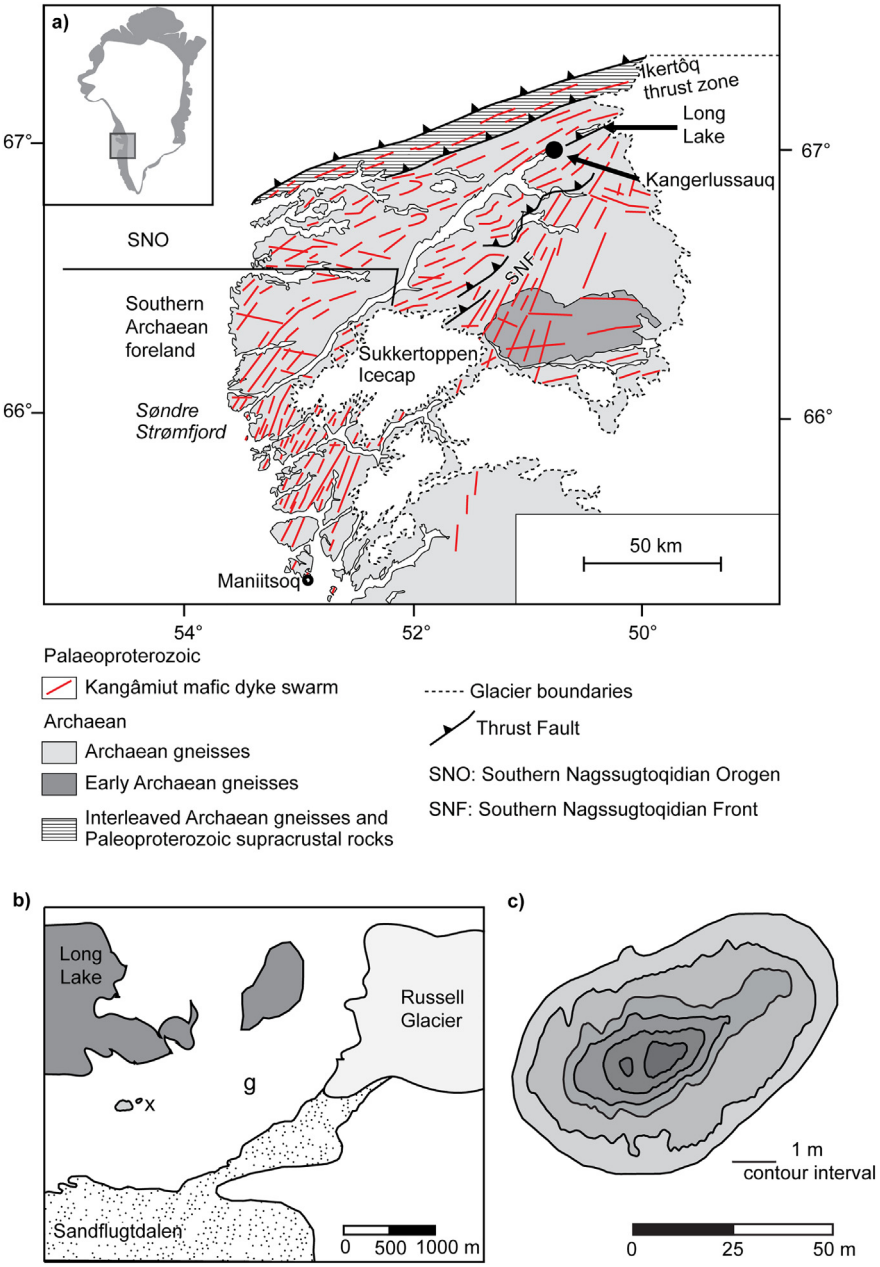

Fig. 1. a) Map indicating location of Kangerlussauq, Greenland and a geologic map of the region showing Proterozoic and Archean bedrock units and orogenic provinces (modified from van Gool et al., 2002b). b) Close up map of the study region between Kangerlussauq and the inland ice margin, showing a major outwash plain/proglacial valley, Sandflugtdalen. X marks the location of EVV Upper lake, and g marks the spot of a nearby gossan deposit. c) Bathymetric map of EVV Upper lake, sampling for this study was done in the deepest central portion of the lake (Z_{max}).

et al., 1999, 2002a, 2002b) with the Kangerlussuag region lying within the southern Nagssugtoqidian orogen (SNO) segment consisting predominantly of reworked gneisses of Achaean age which underwent strong deformation and metamorphism 1.9–1.8 Ga ago (Connelly et al., 2000; van Gool et al., 2002a). Structural fabrics trend east-northeast in the SNO region with folds trending east-west on a kilometer scale and metamorphic grade spanning amphibolite to garnet facies (van Gool et al., 2002b). Also present in the area are the Kangâmiut ultramafic alkaline dyke swarms that have been previously described as kimberlites and lamprolites with varying amounts of pyroxene, olivine, hornblende, pyrite and carbonate minerals (Larsen and Rex, 1992; Jensen et al., 2002). The Kangâmiut dyke swarm was emplaced into the SNO gneisses at ~2.04 Ga ago apparently intruding along pre-existing fracture zones that were present ~200 million years prior to the Nagssugtoqidian Orogeny and were subsequently deformed during collisional folding (Nutman et al., 1999, 2008; Connelly et al., 2000). The mafic dykes are steeply dipping and north-northeast trending in southern Greenland but are folded, foliated, and boudinaged along with their host gneisses in the SNO segment near Kangerlussuaq (van Gool et al., 2002a). The Ikertôq thrust zone is a major geological contact that defines the northern limit of the SNO (Connelly et al., 2000; van Gool et al., 2002a) and marks the northern limit of the Kangâmiut dyke swarm. Fracture features associated with brittle deformation are common in the Kangerlussuaq region, including joints, fissures, cracks and linear veins at scales larger than grain size of the host rocks units.

The ice-free margin of Greenland contains hundreds of thousands of lakes perched on permafrost. Despite their abundance, the majority of the work on Greenlandic lakes focuses on physiochemical limnology and paleolimnology (Anderson et al., 2001, 2008; Anderson and Stedmon, 2007). Our study lake, EVV Upper lake (informal name), lies

within a narrow valley overlying a structural shear zone and extending southwest from the terminal moraine of Russells Glacier to the Søndre Strømfjord near Kangerlussuaq, Greenland (Fig. 1B). The area has continuous permafrost < 50 cm below surface extending down to 300 m depth (Jørgensen and Andreasen, 2007). The ice-cover period lasts from mid-September to mid-June, and lakes in the region are supplied with water mainly through contribution from melting snowpack due to minimal precipitation. EVV Upper lake is the smallest lake in a series of lakes in the valley, with surface area of 0.22 ha and maximum depth of 5.5 m (Cadieux et al., 2016) Further descriptions of EVV Upper lake and work done within it can be found in Goldman et al. (2016), Cadieux et al. (2016, 2017), Colcord et al. (2015), and Thompson et al. (2017).

3. Methods

3.1. Field methods

In order to characterize maximum winter and summer conditions the study lake was sampled in March 2014 (ice-covered) and July 2014 (open-water). The water samples and physiochemical profiles were taken at deepest part of the lake (Z_{max}), which was determined by generating a bathymetric map (Fig. 1D; Cadieux et al., 2016). Water samples and measurements were taken from a backpack-able Alpaca Raft (Anchorage Alaska, USA) during open-water conditions, and by auguring a 30 cm hole in the ~2 m of ice at Z_{max} under ice-cover conditions. Water samples were collected at 0.5 to 1.0 m intervals using an electric submersible pump and were stored in acid-washed and ultrapure water (18.2 MΩ) rinsed high-density polyethylene Nalgene bottles. Dissolved oxygen (DO, μM), pH, temperature (T, °C), and oxidation-redox potential (ORP, mV) were all measured with a YSI 6092 Data Sonde (Yellow Springs Inc., Yellow Springs, OH, USA). A LiCor LI193 Spherical Quantum Sensor (Li-Cor Inc., Lincoln, NE, USA) was used to measure photosynthetically active radiation (PAR, $\mu mol\, m^{-2}\, s^{-1}$) attenuation with depth in the water column. All samples collected for major cation/anion analyses were filtered within 24 h of field collection using a series of Whatman glass fiber filters (0.7 μm) and Millipore membrane filters (0.2 μm) and stored in high-density polyethylene Nalgene bottles and kept frozen until analysis.

Lake sediments were collected using a modified gravity coring device either deployed off the Alpaca raft in open-water conditions or through the augured hole during ice-covered conditions. Sediment cores were capped, sealed, and taken to the field laboratory at KISS (Kangerlussuaq International Science Station) and stored in a freezer at −20 °C. Sediment cores were transported frozen back to our research labs at Indiana University where they sectioned within a N_2-purged glove bag. Extreme care was taken to only sample internal parts of the core that had not come in contact with the core liner to minimize potential for contamination from lake waters and any oxidation that may have happened during coring/transport. Lake sediment samples were then placed with a vacuum freeze drying apparatus to remove all water from samples prior to acid-volatile and chromium reducible sulfide analyses were performed on them. Additionally, gossan samples were extracted from excavated soil pits dug to 40 cm, the depth at which permafrost was reached, and fresh samples were taken every 5–10 cm from the surface down the sidewall of the pit.

3.2. Laboratory methods

Major cation/anion concentrations were determined using a Dionex ICS 2000 Ion Chromatograph using a CS12A analytical cation column, CSRS 300 4 mm suppressor, and 20 mM methanesulfonic acid eluent for cations (corresponding Lower Detection Limit (LDL): Na^+ = 1.2; NH_4^+ = 0.5; K^+ = 0.2; Mg^{2+} = 3.5; Ca^{2+} = 7.1 μM) and an AS11-HC analytical anion column, ASRS 4 mm suppressor and 30 mM potassium hydroxide eluent for anions (LDL; Fl^- = 0.7; Cl^- = 4.0; NO_2^- = 0.6; SO_4^{2-} = 0.9; NO_3^- = 0.2 μM).

Total dissolved sulfide concentrations [ΣH_2S] in the water column were determined gravimetrically by precipitating $H_2S_{(aq)}$ and $HS^-_{(aq)}$ as cadmium sulfide (CdS) precipitate. In the field 10 l of water were collected at desired sample intervals into acid-washed and ultrapure water rinsed Nalgene carboys, containing 200 ml of supersaturated cadmium chloride ($CdCl_2$) solution (Szynkiewicz et al., 2009). Water samples were then centrifuged to separate the CdS precipitate from the remaining water sample. An excess amount of a supersaturated barium chloride ($BaCl_2$) solution was then added to the remaining water samples to precipitate dissolved sulfate as barite ($BaSO_4$) over a 72 h period. The $BaSO_4$ was then rinsed and centrifuged multiple times with ultrapure water to remove chloride salts, and then dried overnight at 80 °C prior to isotopic analysis. The precipitated CdS was then extracted using an acid-volatile sulfide (AVS) technique (e.g., Brüchert and Pratt, 1996; Lefticariu et al., 2006; Young et al., 2013) by placing the solid into an N_2-purged flask and reacted with hot 6 N HCl for ~3 h. The evolved H_2S was carried, via flowing N_2, through a buffer solution (0.1 M sodium citrate solution adjusted to pH 4) into a 0.1 M $AgNO_3$ solution where it was precipitated as silver sulfide (Ag_2S). The Ag_2S is then filtered, rinsed, and dried onto a baked 0.22 μm quartz-fiber filter that is saved for sulfur isotopic analyses. Sulfide concentrations were then determined by the gravimetric yields of collected Ag_2S, and assuming a stoichiometry of H_2S/HS^-: Ag_2S of one. Minimum detection limits using cadmium precipitation are 0.5 μM, based upon laboratory experiments with pure H_2S and water.

Approximately 5 g freeze dried gossan samples were rinsed with excess ultrapure (18 MΩ) water for 10 min then centrifuged, and dissolved sulfate was then extracted from the water using procedure above for barite (water soluble sulfate). The remaining gossan residue was next extracted using the AVS technique described above. After the AVS extraction the acidic superannuate solution was separated from insoluble residue using centrifugation and then acid-soluble sulfate (AS-SO_4) was extracted using barite extraction described above. The final insoluble residue was subjected to a chromium-reducible sulfide (CRS) technique to extract predominantly sedimentary pyrite (e.g., Brüchert and Pratt, 1996; Lefticariu et al., 2006).

Homogenized $BaSO_4$ and Ag_2S powders were loaded into tin capsules with excess V_2O_5 and analyzed for of their $\delta^{34}S$ content by SO_2-method using a Costech Elemental Analyzer coupled to a Thermo Delta V Plus isotope ratio mass spectrometer via a Conflo IV split interface. Calibration of our samples via SO_2-method was done based on laboratory standards calibrated relative to the IAEA S-1 standard ($\delta^{34}S$, −0.30‰) and NBS-127 ($\delta^{34}S$, +20.3‰). All results are reported in standard delta (δ) notation with units reported as parts per thousand or permil (‰) relative to the standard VCDT [Vienna Canyon Diablo Troilite] for $\delta^{34}S$:

$$\delta^{34}S = [(^{34}S/^{32}S)_{sample}/(^{34}S/^{32}S)_{VCDT} - 1] \times 1000 \quad (1)$$

Analytical reproducibility was better than ± 0.2‰ for standards and duplicate samples all of which were analyzed in the Stable Isotope Research Facility (SIRF) at Indiana University. In addition to Table 1 all sulfur concentration and isotopic data generated for this study are reported in Appendix Table in the supplementary material file.

4. Results

4.1. Water column physiochemistry

During, open-water conditions, EVV Upper lake was thermally stratified ($\Delta T = T_{0m} - T_{zmax}$) with $\Delta T \approx 9$ °C, and under ice-cover conditions the lake was isothermal with $\Delta T < 0.5$ °C (Fig. 2). The changes in pH during open-water conditions co-varied with temperature and chemical composition (i.e., dissolved O_2, redox potential; see section below) of the lake shifting from a pH of 7.8 at the surface to 6.8

Table 1
Sulfur geochemical data for EVV Upper lake, southwestern Greenland. See Sections 3.1 and 3.2 for description of field and laboratory methods.

Water column depth (m)	$[SO_4]$ (μM)	$[H_2S]$ (μM)	$\delta^{34}S_{SO4}$ (‰)	$\delta^{34}S_{H2S}$ (‰)	ε_{SR}[a] (‰)	Sulfur fraction[b]	$\delta^{34}S_{AVS,CRS}$ (‰)	$\Delta^{34}S$[c] (‰)	AVS-S, pyrite-S (wt%)
Ice-covered conditions									
2.5	600.8	6.4	20.2	−22.2	42.4				
3.0	522.3	13.0	23.6	−22.2	45.8				
3.5	592.5	23.8	15.4	−22.2	37.6				
4.0	541.3	23.9	22.3	−22.4	44.7				
4.5	552.9	30.7	19.7	−21.4	41.1				
5.0	517.5	25.5	19.5	−20.9	40.4				
0–2 cm within sediment						AVS	1.2 (1)		0.01
0–2 cm within sediment						CRS	−8.2 (5)		0.60
								26.6	
Open-water conditions									
1.0	335.7	b.d.	16.2	b.d.	–				
2.0	328.6	0.3	16.1	−7.8	23.9				
3.0	335.6	0.4	16.1	−7.5	23.6				
3.5	333.3	0.2	16.0	−9.1	25.0				
4.0	338.3	0.2	15.6	−7.6	23.2				
5.0	354.2	29.0	26.0	6.3	19.7				
0–2 cm within sediment						AVS	3.1 (2)		0.03
0–2 cm within sediment						CRS	3.2 (2)		0.79
								13.0	

[a] Calculated as sulfur isotopic difference between water column sulfate and sulfides.
[b] Sulfur fraction abbrevations: AVS, acid-volatile sulfides; CRS, chromium reducible sulfides.
[c] Calculated as sulfur isotopic difference between surficial sulfate and mean of sedimentary sulfides.

at 4.5 m depth. Under ice-cover conditions pH was 6.9 and stable throughout the lake, also mirroring the overall temperature and chemical composition of EVV Upper lake (Fig. 2). PAR values of 910 μmol $m^{-2} s^{-1}$ were observed in the surface waters during open-water conditions but quickly decreased in the upper 2 m of the water column to values < 50 μmol $m^{-2} s^{-1}$ and < 10 μmol $m^{-2} s^{-1}$ below 3 m depth. Under ice-covered conditions PAR values for the lake were all < 2 μmol $m^{-2} s^{-1}$(Fig. 2).

A clinograde DO profile was observed in under open-water conditions, wherein the surface waters exhibited saturated levels that are within equilibrium with the atmosphere but decrease with depth (Fig. 4). An anoxic (DO ≤ 5 μM) water column was detected below 4 m water depth during open-water conditions and under ice-cover, the water was completely anoxic. Oxidation-redox potential (ORP) profiles for both open-water and ice-covered conditions co-varied with DO levels; during open-water conditions ORP values shifted from 180 mV at 3 m to < −200 mV at 4.5 m corresponding to the large drop in DO levels at the same water depths. During ice-covered conditions only water at the ice cover–lake water interface was at 101 mV and then all measurements below that were < −200 mV. Overall, the thermal structure and DO profiles are consistent with previous observations for EVV Upper lake (Cadieux et al., 2016, 2017). All physiochemical data presented in this paper are reported within Appendix Table within the Supplementary data.

Under both open-water and ice-covered conditions, cation abundance follows $Ca2+ > Mg2+ > Na+ > K^+$, and anion abundance follows $Cl^- > SO_4{}^{2-} > NO_2{}^- > NO_3{}^-$ (Fig. 3) consistent with other dilute lakes in the region (Cadieux et al., 2017). All ion

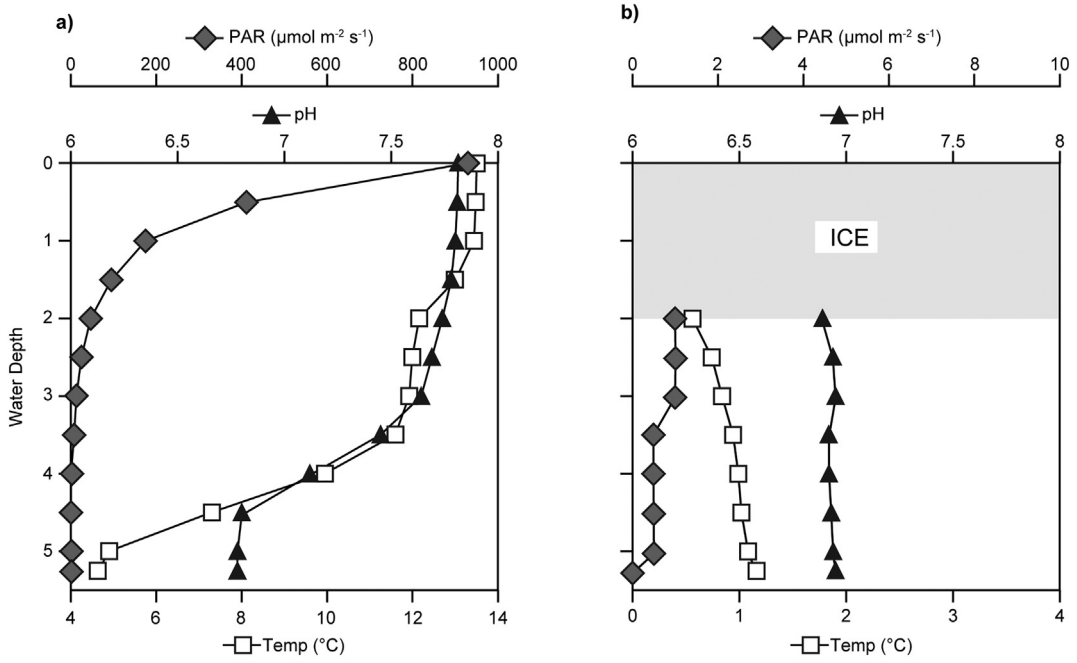

Fig. 2. Profiles of temperature (T), pH, and photosynthetically active radiation (PAR) under open-water (a) and ice-covered (b) conditions in EVV Upper lake.

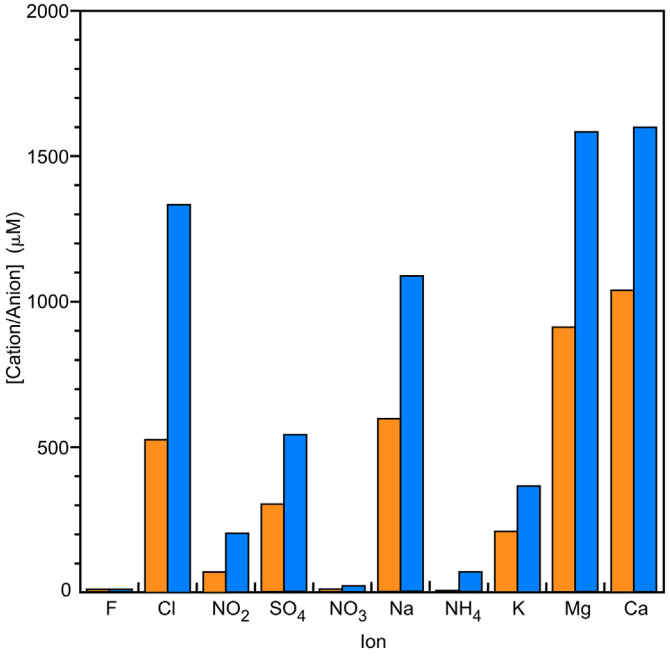

Fig. 3. Median values of major anion and cations in water samples from EVV Upper lake collected under both open-water (orange) and ice-covered (blue) conditions. (For interpretation of the references to color in this figure legend, the reader is referred to the web version of this article.)

concentrations were greater under ice-covered conditions than open-water conditions, ranging from increasing 30% (F^-) to 94% (NH_4^+), with an average increase of 52%.

4.2. Concentrations of Sulfur (SO_4, and ΣH_2S) and isotopic compositions

Similar to other ions, sulfate concentrations were greater under ice-covered conditions than open-water conditions, with average sulfate concentrations at 554.6 ± 35.1 μM and 337.6 ± 8.8 μM respectively. During open-water conditions there were no marked changes in sulfate concentration regardless of depth, unlike ΣH_2S concentrations which showed values of < 1μM above the chemocline (~4 m depth) and 29 μM below the chemocline (Fig. 4B). The marked increase in [ΣH_2S] was coincident with very low DO levels (anoxic conditions) and ORP values < −200 mV. The dissolved sulfate and sulfide $\delta^{34}S$ values exhibited rapid ^{34}S enrichments across the chemocline when compared to the overlying surface waters (Fig. 4C). Open-water $\delta^{34}S_{SO4}$ values were very stable at +16.0 ± 0.2‰ in the upper 4 m of the lake, and increased below the chemocline to +26.0‰. Corresponding $\delta^{34}S_{H2S}$ values exhibited a similar pattern with respect to the chemocline, with stable values of −8.0 ± 0.7‰ above 4 m and a sharp increase to +6.3‰ below. The average sulfur isotopic offset ($\varepsilon_{SR} = \delta^{34}S_{SO4} - \delta^{34}S_{H2S}$) above the chemocline was 24‰, and decreased slightly below the chemocline to 20‰.

Under ice-covered conditions, sulfate concentrations in EVV Upper lake were 600.8 μM just below the ice-cover and decreased with depth to 517.5 μM at 5 m. In contrast, sulfide concentrations increased with depth from 6.4 μM at 2.5 to values of > 20 μM below 3 m depth. Relative to open-water conditions the $\delta^{34}S_{SO4}$ and $\delta^{34}S_{H2S}$ values throughout the water column were more stable and consistent, with $\delta^{34}S_{SO4}$ values +20.1 ± 2.8‰ and $\delta^{34}S_{H2S}$ values of −21.9 ± 0.6‰. The ε_{SR} during ice-coved conditions was stable throughout the water column at 42.0‰, and approximately twice that of open-water conditions. These apparent fractionations are well within the range of modern aquatic systems and pure laboratory cultures of MSR (e.g., Canfield et al., 2010; Sim et al., 2011a, 2011b and references therein).

4.3. Sedimentary sulfides in EVV Upper lake and nearby gossan deposit

Solid-phase sulfides were extracted (AVS and CRS) from shallow cores taken under chemocline during both open-water and ice-covered conditions (Table 1; Fig. 5). We acknowledge that the CRS extraction is an operationally defined pool of polysulfides, of which pyrite is the predominant mineral that comprises it in most sedimentary samples although other metastable sulfide minerals can contribute to this pool (e.g., greigite, mackinawite). The $\delta^{34}S_{AVS}$ and $\delta^{34}S_{pyr}$ were nearly identical during open-water conditions with values at 3.1‰ and 3.2‰, respectively. However, during ice-covered conditions $\delta^{34}S_{AVS}$ and $\delta^{34}S_{pyr}$ varied from each other (~9‰ offset) with values at 1.2‰ and −8.2‰ respectively. In a nearby gossan deposit associated with weathering of underlying Paleoproterozoic mafic dikes, sulfur was extracted and analyzed from excavated soil pits to a depth of 40 cm. The average abundance of water-soluble sulfate, acid soluble sulfate, and pyrite were 100 ppm, 7 wt%, and 10 ppm, respectively. The $\delta^{34}S$ values of water soluble sulfate, acid soluble sulfate, and pyrite ranged from −0.7‰ to +2.0‰ (mean = 1.5‰), −1.2 to +1.0‰ (mean = 0.7‰), and + 1.3‰ to +6.7‰ (mean = 2.6‰) respectively (Fig. 6). The $\delta^{34}S$ values of all water-soluble sulfate and pyrite, were higher than acid soluble sulfate.

5. Discussion

5.1. Sulfur sources to EVV Upper lake

Sulfate concentrations in EVV Upper lake are an order of magnitude higher than other nearby small lakes in the same valley, the closest being only ~100 m west with [SO_4] ranging from 6 to 45 μM (Cadieux et al., 2016, 2017). As previously described, EVV Upper lake is part of a series of lakes that are within a narrow (~1 km) valley overlying a structural shear zone and nearby thrust fault that extends from Russell Glacier to Søndre Strømfjord (Fig. 1A; van Gool et al., 2002b). The underlying bedrock in the valley consists largely of folded metasediments and mafic dykes, and chemical dissolution of mineralized mafic dykes, metapelites, metasiltstones, and metargillites (Nutman et al., 1999; van Gool et al., 2002b) are the most likely sources of sulfate to EVV Upper lake. A local outcrop of the Paleoproterozoic mafic dyke and associated gossan deposit overlying record $\delta^{34}S$ values from to −1.2‰ to +6.7‰ (Fig. 6) well within the range of a mantle/hydrothermal S sources (Bottrell and Newton, 2006). Although surficial weathering and transport of sulfur from this particular mafic dyke outcrop may not be the source of sulfate to EVV Upper lake, the north-northeast trend of the dyke and associated structural features align well with axis of this narrow valley and EVV Upper lake. Therefore, it is possible that a mafic dyke bedrock is directly underlying EVV Upper lake and/or a majority of its catchment in this part of the valley. Peletic metasediments are another possible source of sulfate to EVV Upper lake they are not necessarily favored as low-sulfide abundance, quartzites and quartzofeldspathic metasediments are more common in our study region, furthermore the largest volumes of metasedimentary rocks are found within the Ikertôq Thrust Zone (Nutman et al., 1999; van Gool et al., 2002a, 2002b), which is ~10–15 km north of our study area. Sulfide minerals (i.e., pyrite) from these Paleoproterozoic–late Archaean metasedimentary rocks could have a range of possible $\delta^{34}S$ values from ~−20‰ to ~+20‰ (e.g., Canfield, 2005).

As mentioned above bedrock in the study area is highly fractured and a major thrust fault has been mapped near our study area (Fig. 1), however there are no indications of recent hydrothermal activity in the region that could act as a potential pathway for fluid flow into the lake catchment. Furthermore, the region has continuous permafrost (Jørgensen and Andreasen, 2007), which makes it highly unlikely that any significant and active groundwater reservoirs are contributing to EVV Upper lake. Interestingly, the average EVV Upper lake $\delta^{34}S_{SO4}$ is ≈19‰ which is similar to that of modern day seawater,

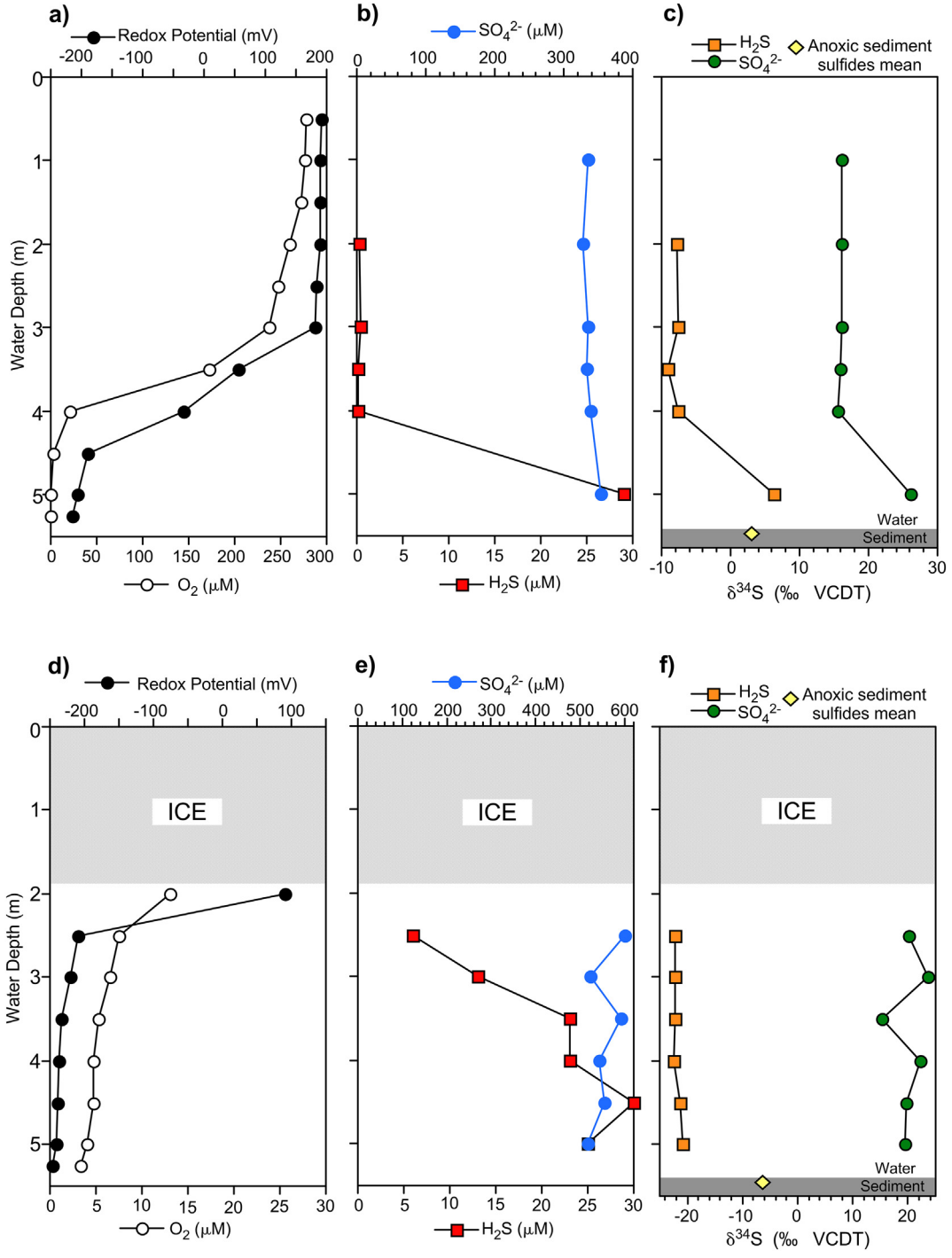

Fig. 4. Vertical geochemical profiles for EVV Upper lake. Plots of dissolved O_2 and redox potential (a, d). Plots of sulfate and sulfide concentrations (b, e). Plots of water column $\delta^{34}S_{SO4}$ and $\delta^{34}S_{H2S}$, along with mean $\delta^{34}S$ value of sedimentary sulfides from uppermost sediments (c, f).

$\delta^{34}S_{SO4}$ = 21‰ (Rees et al., 1978). However, our study area is over 100 km inland from the western coast of Greenland, and precipitation in the Kangerlussuaq region is low (< 150 mm/yr) making any marine sulfate delivery source (e.g., DMS, DMSP, DMSO) unlikely. Therefore, geothermal fluids, groundwater, and marine-atmospheric inputs are not favored sources of sulfur to EVV Upper lake at this time.

Many of these scenarios, or a combination of them, may be plausible sources of sulfur to EVV Upper lake and other small lakes in the region. However, the most parsimonious sulfate source is via chemical dissolution of the mafic dykes and/or metasedimentary formations that outcrop within the valley and/or underlie the lake, catchment regolith, and surrounding permafrost. Current $\delta^{34}S$ values of dissolved sulfate in the lake could be derived from mixing of the two potential bedrock sources (mafic dykes −1.2 to 6.7‰ and metasedimentary rocks −20 to 20‰) or ^{34}S enrichment of the sulfate reservoir with time as more ^{34}S-depleted sedimentary sulfides are buried. However, our seasonal study of water column $\delta^{34}S_{SO4}$ and $\delta^{34}S_{H2S}$ (Fig. 4) suggests microbial processing and likely overprinting of the original sulfur source material and isotopic composition.

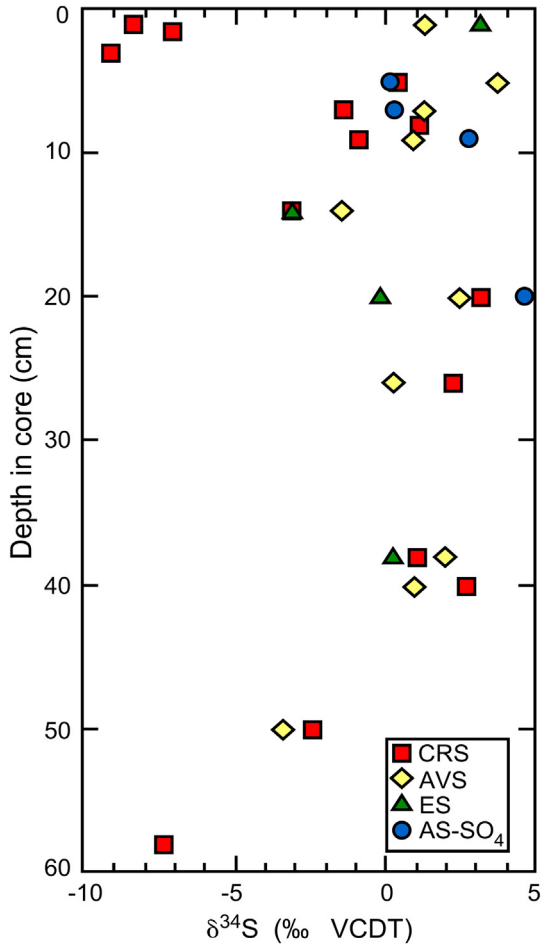

Fig. 5. EVV Upper lake solid phase sulfur isotope data for sediments collected from under euxinic ice-covered conditions. Sequentially extracted phases of sulfur were extracted from each sediment core sample as elemental sulfur (ES), acid-soluble sulfate (AS-SO4), acid volatile sulfides (AVS), and chromium reducible sulfides (CRS).

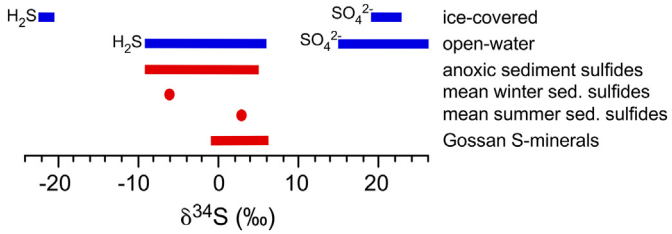

Fig. 6. Range of observed $\delta^{34}S$ values for different pools of sulfur in or nearby EVV Upper lake.

5.2. Water column $\delta^{34}S$ trends

Here we have documented seasonal isotopic variability of microbial processing of sulfur within EVV Upper lake (Fig. 4). During open-water conditions the $\delta^{34}S_{SO4}$ and $\delta^{34}S_{H2S}$ values remain stable throughout the upper 4 m of the water column with a rapid increase in values (10‰ and 14‰, respectively) in the lowermost meter and half of the water column and $\Delta^{34}S$ at ~24‰. While during the ice-covered conditions $\delta^{34}S_{SO4}$ and $\delta^{34}S_{H2S}$ values remain stable throughout the water column and $\Delta^{34}S$ are ~42‰. Sulfur isotopic variability documented within the water column during open-water conditions strongly indicate both a kinetic isotope effect associated with microbial sulfur cycling and a reservoir effect (notable increase $\delta^{34}S_{SO4}$ and $\delta^{34}S_{H2S}$ values with depth) govern the $\delta^{34}S_{SO4}$ and $\delta^{34}S_{H2S}$ trends, while under ice-cover ε_{SR} is dominant control on dissolved sulfate and sulfide within EVV Upper lake. In addition to $\delta^{34}S$ values there are broad correlations ($R = 0.67$, p-value = 0.44 for open-water; $R = 0.89$, p-value = 0.03 for ice-cover) observed with $[\Sigma H_2S]$ increasing with depth below the chemocline under open-water and ice-covered conditions (Fig. 4) indicating that MSR is the primary microbial pathway affecting sulfur in this lake, with perhaps some inputs from sulfide oxidation (see further discussion below).

We use our measured $\delta^{34}S_{SO4}$ and a Rayleigh distillation model to calculate the average ε_{SR} in the euxinic portions of the Upper EVV lake water column:

$$\delta^{34}S_{SO4,d} - \delta^{34}S_{SO4,surf} = \varepsilon \ln(fSO_4^{2-}{}_{,d}) \quad (2)$$

where $\delta^{34}S_{SO4,\,d}$ is the sulfur isotopic composition of sulfate measured at the water column depth, $\delta^{34}S_{SO4,\,surf}$ is the average sulfur isotopic composition of sulfate measured in the surface waters (≤1 m), $fSO_{4,d}^{2-}$ is the fraction of sulfate remaining at depth, and ε is the fractionation value ε_{SR} (after Mariotti et al., 1981). Rayleigh plots of the euxinic portions of Upper EVV lake under ice-cover and open-water conditions reveal linear relationships with natural log of the fraction of sulfate remaining versus the $\delta^{34}S_{SO4}$ measured at each depth (Fig. 7). Using the slope of the line for ice-covered conditions an average fractionation of 45‰ is calculated, which is very close to the observed ε_{SR} of 42‰. Although we cannot definitively rule out other microbial processes cycling S (e.g., sulfide oxidation, sulfur disproportionation), the y-intercept value of 15.7‰ is very near to the measured $\delta^{34}S_{SO4,\,surf}$ values (16‰) and moderate–strong linear correlation ($R = 0.78$, p-value = 0.06) support the assumption that EVV Upper lake is a closed system under ice-covered conditions whereby sulfate concentration and $\delta^{34}S_{SO4}$ values are primarily controlled by MSR. The open-water Rayleigh model value calculated for average fractionation is notably much

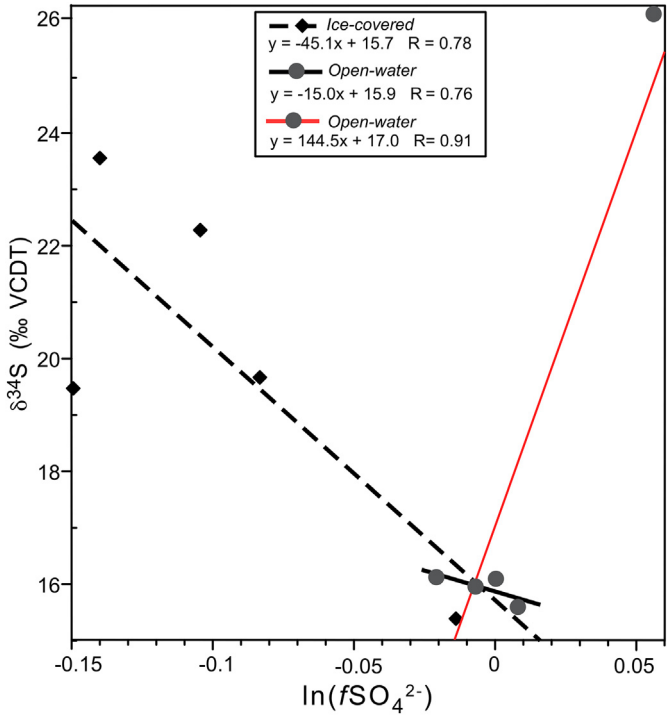

Fig. 7. Rayleigh plots of the natural log of the fraction of sulfate remaining at each depth versus $\delta^{34}S_{SO4}$ for open-water and ice-covered conditions. Please note that the two Rayleigh models for open-water conditions above the chemocline (black line) and with data below chemocline included (red line). (For interpretation of the references to color in this figure legend, the reader is referred to the web version of this article.)

larger than under ice-covered conditions when considering the water column above the chemocline, 144‰ versus observed ε_{SR} of ~24‰, and this calculated fractionation is well outside of the known range during MSR. This disparate Rayleigh model value may result from the small increase in sulfate concentration below the chemocline rather than the an expected decrease in sulfate within a closed system primarily controlled by MSR and a reservoir isotope effect. The y-intercept value calculated (17.0‰) is very near the $\delta^{34}S_{SO4,\ surf}$ values, and the strong linear correlation ($R = 0.91$, p-value = 0.06) support broadly closed-system behavior in the euxinic portion of the water column with MSR being a significant control on $\delta^{34}S_{SO4}$ values in the water column under open-water conditions. Interestingly, if only the water-column values above the chemocline are considered in the Rayleigh model then the average fractionation value obtained is notably smaller than under ice-covered conditions, 15‰ versus observed ε_{SR} of ~24‰, and this offset is consistent with other studies of sulfur isotope systematics in open-water aquatic systems in which these models underestimate observed fractionations (e.g., Goldhaber and Kaplan, 1980; Gomes and Hurtgen, 2013; Crowe et al., 2014b). The y-intercept value is indistinguishable from the $\delta^{34}S_{SO4,\ surf}$ values, and the moderate-strong linear correlation ($R = 0.76$, p-value = 0.13) support closed-system behavior in the euxinic portion of the water column with MSR being a significant control on $\delta^{34}S_{SO4}$ values in the water column under open-water conditions.

Two of the Rayleigh modeled and the observed ε_{SR} values are well within the range of fractionations values known to occur during MSR, up to 70‰ in laboratory and natural environments (Habicht and Canfield, 1996; Canfield et al., 2000; Rudnicki et al., 2001; Wortmann et al., 2001; Sim et al., 2011a, 2011b). Furthermore, our seasonal $\delta^{34}S$ systematics of this lake show evidence of suppression of MSR fractionation due to declining [SO_4^{2-}] from ice-covered to open-water conditions. While sulfate reservoir size is known to place constraints on kinetic isotope fractionations (Kaplan and Rittenberg, 1964; Habicht et al., 2002; Kah et al., 2004), other environmental factors such as cell-specific MSR rates, reactive carbon substrate, nutrients, and microbial community structure can also be expressed in $\delta^{34}S$ fractionations (Harrison and Thode, 1958; Kemp and Thode, 1968; Postgate, 1984; Brüchert et al., 2001; Habicht and Canfield, 1996; Canfield, 2001; Lyons et al., 2004; Sim et al., 2012; Leavitt et al., 2013). Chemical reaction rates decrease with lowered temperatures, including microbial processes such as aerobic respiration rates (Stanley, 2010; Finnegan et al., 2012). The thermodynamic relationship of temperature and respirations rates is expressed in the sizable increases in dissolved organic carbon concentrations from 48 to 75 mg L^{-1} under open-water conditions to 65–103 mg L^{-1} under ice-covered conditions in EVV Upper lake (Cadieux et al., 2017). When we compare PAR levels in EVV Upper lake to DOC and temperature we see an inverse relationship (900 μmol m^{-2} s^{-1} vs. 0 to 2 μmol m^{-2} s^{-1}) suggesting there was much higher photosynthesis driven productivity in open-water compared to ice-cover conditions. Corresponding respiration rates in EVV Upper lake would have to be higher to explain the lower DOC levels in the open-water conditions and as a result cell-specific MSR rates may likely have been higher (once O_2 and other terminal electron acceptors were depleted). Based upon recent laboratory experiments (Sim et al., 2011a, 2011b) we would expect that the rates of MSR would increase under these documented ice-covered conditions due to the increased availability of labile organic substrates thereby decreasing ε_{SR}. However, our observed ε_{SR} values under ice-covered conditions show a marked increase compared to open-water conditions, suggesting that changes organic carbon substrates were not the dominant control on fractionation between $\delta^{34}S_{SO4}$ and $\delta^{34}S_{H2S}$ in EVV Upper lake. Thus, we suggest that changes in cell-specific MSR rates and sulfate concentrations are the predominant factors that has influencing MSR in EVV Upper lake and furthermore the change in expression of $\delta^{34}S$ fractionation observed between open-water and ice-covered conditions.

While MSR is a critical microbial process cycling sulfur in EVV Upper lake and thus impacting the observed $\delta^{34}S$ trends in the water-column and sediments, this kinetic isotope effects alone cannot explain the $\delta^{34}S$ trends observed within the water column during open-water conditions. In addition to kinetic isotope effects imparted during MSR a reservoir effect is observed and associated with the low sulfate concentrations in EVV Upper lake influencing the $\delta^{34}S_{SO4}$ and $\delta^{34}S_{H2S}$ at depth in the water column. Low sulfate concentrations under open-water stratified conditions allow for MSR to impart moderate fractionations within the water column that show ^{34}S enrichment with depth as the residual sulfate pool becomes isotopically heavier. The $\delta^{34}S_{H2S}$ at depth also becomes enriched, tracking $\delta^{34}S_{SO4}$, due to the ^{34}S enrichment of the reactant sulfate pool with depth (i.e., Gomes and Hurtgen, 2013). Additionally, ^{34}S enrichment has been shown to occur more rapidly in low-sulfate systems than in high-sulfate depositional environments (e.g., Gomes and Hurtgen, 2015).

5.3. Linkage between water-column S cycling and the lake sediments

The variation of $\delta^{34}S_{H2S}$ with depth is important as $\delta^{34}S_{pyr}$ are sensitive to the location where pyrite formation occurs (e.g., throughout anoxic waters, sediment-water interface, and/or within sediments) and availability of Fe^{2+} (Lyons, 1997). A recent model for pyrite formation in stratified systems, based upon a compilation of $\delta^{34}S$ data from modern euxinic bottom waters, where both kinetic and reservoir isotope effects are impacting $\delta^{34}S$ values predicts that primary location of pyrite formation significantly affects $\delta^{34}S_{pyr}$ and $\Delta^{34}S$ calculated from them (i.e., Gomes and Hurtgen, 2015). It is important to note that solid phase sedimentary sulfides are time averaged and don't solely reflect the sulfide forming at the time of sampling, instead could reflect sulfides forming throughout the year in the water-column and/or sediments. Furthermore, these $\delta^{34}S$ values for the upper 2 cm are time averaged as recent age models for sedimentation rates in EVV Upper lake are 17 cm/kyr with the upper 2 cm representing 120 ± 25 yrs. (Colcord et al., 2015). In EVV Upper lake, the open-water mean sedimentary sulfides $\delta^{34}S$ value for the upper 2 cm is +3.1‰, which is isotopically lighter than $\delta^{34}S_{H2S}$ values at ~0.5 m above the sediment-water interface but heavier than $\delta^{34}S_{H2S}$ values near the chemocline. Additionally, the $\Delta^{34}S$ value in the sediment is 13‰, which is lower than the ε_{SR} value of 23‰ (Fig. 4, Table 1). When comparing our sulfur isotopic data just described for open-water conditions to model predictions (i.e., Gomes and Hurtgen, 2015) and assuming closed-system behavior in EVV Upper lake, it appears that during open-water conditions pyrite was primarily forming throughout the euxinic water column and near the sediment-water interface. During ice-covered conditions the mean sedimentary sulfides $\delta^{34}S$ value for upper 2 cm is −6.3‰ and is isotopically much heavier than all water-column $\delta^{34}S_{H2S}$ values (mean value, −21.9‰), and the $\Delta^{34}S$ value of 26.6‰, which is lower than ε_{SR} values of 42‰ from the water column. These water column $\delta^{34}S$ trends, $\delta^{34}S_{pyr}$, ε_{SR}, and $\Delta^{34}S$ values all suggest the influence of a reservoir effect was minimal to non-existent during ice-covered conditions.

The $\delta^{34}S$ values of sedimentary sulfides, collected under both ice covered and open-water conditions, in the upper 2 cm of the core (Fig. 5) do not reflect exclusively kinetic isotope effects associated with MSR as seen in the water-column $\delta^{34}S$ trends. Additionally, pyrite formation within the sediments is a process that contributes to $\delta^{34}S$ of sedimentary sulfides within the upper 2 cm of the core, however the rate at which this process happens and its fractionation variability is not likely to change seasonally due to continuous reducing conditions, supply of organic matter, sulfate, and Fe^{2+} to the system. To assess the potential for the $\delta^{34}S$ values of sedimentary sulfides in these uppermost anoxic sediments to represent admixtures of pyrite formed from different seasonal water-column conditions theoretical sedimentary sulfide (FeS_2) $\delta^{34}S$ values were calculated with a simple sulfur isotope mass balance model using the following equation:

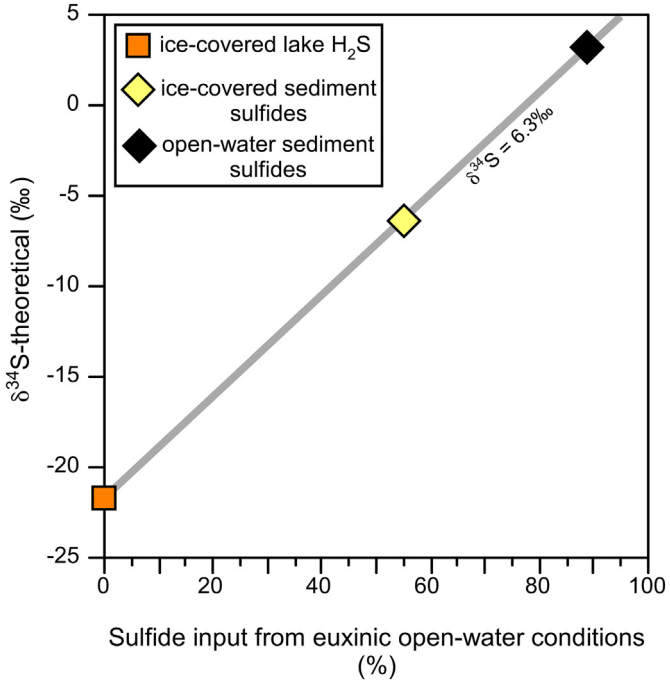

Fig. 8. Sulfur isotope mass balance model calculated for mixing of pyrite formed under open-water euxinic conditions and under ice-covered euxinia. With mean $\delta^{34}S$ values of sedimentary sulfides recovered from uppermost anoxic lake sediments under both open-water and ice-covered conditions.

$$\delta^{34}S(FeS_2)_{pyrite,0-2\,cm} = r_1 * \delta^{34}S(H_2S)_{open-water\ euxinia} + r_2 * \delta^{34}S(H_2S)_{ice-covered\ euxinia} \quad (3)$$

where r_1 and r_2 are parameters that represent the amount of pyrite formed from open-water and ice-covered euxinic EVV Upper lake seasonal conditions, respectively. Mean water column $\delta^{34}S_{H2S}$ values for ice-covered conditions and below chemocline $\delta^{34}S_{H2S}$ values for open-water conditions were used for our calculations. The theoretical mixing model presented here (Fig. 8) shows that pyrite formed during euxinic open-water conditions can account for 50–55% of the sedimentary sulfides in the upper 2 cm anoxic sediments collected under ice-cover. While only 5–10% of the sedimentary sulfides in the upper 2 cm anoxic sediments collected under open-waters can be accounted for by pyrite formed during previous ice-covered euxinic conditions. Our modeling and geochemical data suggests that the Gomes and Hurtgen (2015) euxinic systems model is largely applicable to our observed open-water euxinic conditions, but their model cannot explain our observed $\delta^{34}S$ values, calculated $\Delta^{34}S$ and ε_{SR} under ice-cover conditions. Seasonal recycling of pyrite formed under ice-cover via oxidation from lake overturn during spring ice-break up and mixing conditions may be responsible for the very low percentage of sedimentary sulfides that can be accounted for in the theoretical model. Alternatively, the ice-covered burial flux of pyrite may have undergone further recycling (reductive dissolution and oxidation) within the sediments–pore waters after subsequent burial and exchange became limited with overlying lake waters. While our theoretical model doesn't account for any sulfur isotope fractionations that seasonal abiotic and/or biotic oxidation pathways might have on the sedimentary sulfides, these isotope effects are small, ≤5‰ (e.g., Zerkle et al., 2009 and references therein). Any sedimentary sulfide re-oxidation process operating in these lake sediments likely involved both DO and highly reactive iron (Fe_{HR}), while iron speciation was not measured for this study AVS and CRS concentrations (0.6–0.8 wt%) give us a reasonable indication that corresponding Fe_{py} (one species of Fe_{HR}) were high and a large fraction of Fe_{HR} was reduced iron (e.g., Raiswell and Canfield, 2012). The small isotope effect associated with sulfide oxidation could explain the small (3‰) offset between open-water euxinic $\delta^{34}S_{H2S}$ and $\delta^{34}S_{pyr}$ values, but cannot fully account for the 13‰ offset of $\delta^{34}S_{H2S}$ and $\delta^{34}S_{pyr}$ values under ice-covered conditions. Furthermore, this sulfide re-oxidation process is likely in part responsible for the isotopically light AS-SO_4 (relative to water column $\delta^{34}S_{SO4}$) fractions within the upper 10–20 cm of the core sediments. In general, the trend towards heavier $\delta^{34}S$ values (−9‰ to 3‰) in the upper 20 cm (Fig. 5) of the core suggest more sedimentary sulfides were forming below sediment-water interface as pore waters become more restricted and continued MSR drives pore fluids towards greater ^{34}S enrichment (e.g., Turchyn et al., 2006; Feng and Roberts, 2011). The trend back to lighter $\delta^{34}S$ values below 40 cm in the core could reflect periods during earlier lake history where there was very limited MSR activity within the sediments perhaps due to limitations in sulfate, organic matter, iron, or other nutrients.

5.4. Comparison with other modern euxinic systems

EVV Upper lake $\delta^{34}S_{H2S}$, $\delta^{34}S_{pyrite}$, and calculated $\Delta^{34}S$ values are similar to other modern low-sulfate (0.03–8.5 mM) euxinic systems (e.g., Gomes and Hurtgen, 2015 and references therein). Similarly, $\Delta^{34}S$ values calculated as $\Delta^{34}S_{H2S}$ ($\Delta^{34}S_{H2S} = \delta^{34}S_{sulfate} - \delta^{34}S_{H2S}$) and $\Delta^{34}S_{sed.\ sulfides}$ ($\Delta^{34}S_{sed.\ sulfides} = \delta^{34}S_{sulfate} - \delta^{34}S_{pyr}$) in EVV Upper lake are most comparable with $\Delta^{34}S$ values at Savoko Lake and Lake Fukami-ike (Ivanov, 1978; Nakagawa et al., 2012). However, the difference between $\Delta^{34}S_{H2S}$ and $\Delta^{34}S_{sed.\ sulfides}$ in EVV Upper lake during open-water versus ice-covered conditions is 10.9‰ and 15.4‰, respectively (Fig. 9), while three of the other low-sulfate euxinic systems with both water-column and sedimentary sulfide $\delta^{34}S$ values measured have offsets that are < 5‰. The offset in calculated $\Delta^{34}S$ values at Savoko Lake is of similar magnitude (13.4‰) but different directionality (i.e., larger $\Delta^{34}S_{sed.\ sulfides}$), and is attributed to a reservoir effect within the lake sediments as groundwater-sulfate diffuses through the sediments becomes ^{34}S-enriched due to MSR and the resulting sulfate entering the

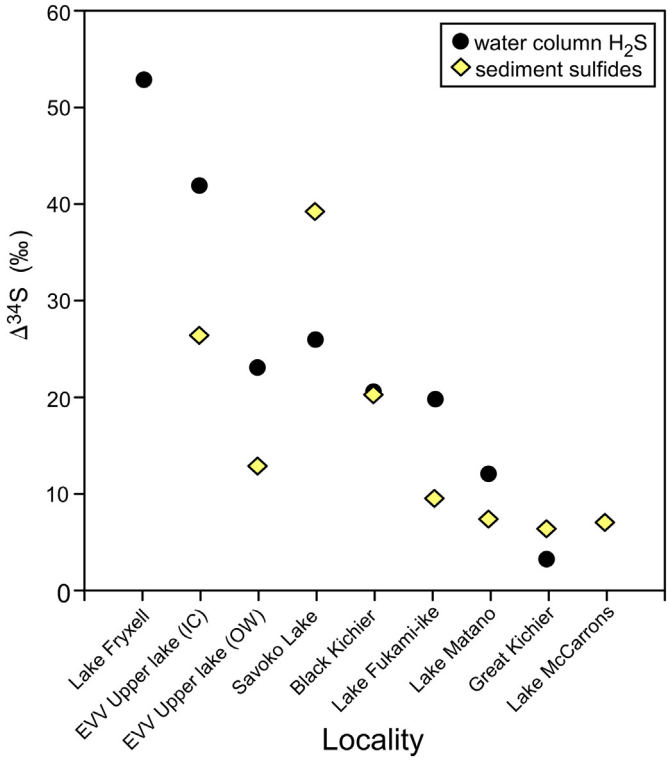

Fig. 9. Comparison of $\Delta^{34}S$ values calculated from $\delta^{34}S_{H2S}$ water column profiles and mean $\delta^{34}S$ values of sedimentary sulfides for modern low-sulfate euxinic systems (data for other low-sulfate lakes from Gomes and Hurtgen, 2015 and references therein).

karst lake system has a higher $\delta^{34}S$ values (Ivanov, 1978). The offset in calculated $\Delta^{34}S$ values at Lake Fukami-ike is ~10.2‰, and similar to Savoko Lake, and groundwater is also the major source of sulfate to this system as well (Nakagawa et al., 2012). Furthermore, seasonal changes in microbial sulfur cycling have been documented within Lake Fukami-ike using both sulfur isotopic and microbiological analyses. Similar to EVV Upper lake, a reservoir effect in addition to kinetic isotope effect associated with MSR ($\Delta^{34}S_{H2S}$ = 11–56‰) was documented in Lake Fukami-ike during early lake stratification stages (Nakagawa et al., 2012).

There are very few ice-covered lake systems that have been previously studied using $\delta^{34}S$ analyses to investigate microbial sulfur cycling that could be compared to EVV Upper lake. A recent study of Lake Fryxell, a perennially ice-covered lake in the McMurdo Dry Valleys, Antarctica document low-sulfate conditions (~1.4 mM) with water column $\Delta^{34}S_{H2S}$ values of 51–55‰ (Saxton et al., 2016). Both sulfate levels and $\Delta^{34}S_{H2S}$ values are higher in Lake Fryxell compared to EVV Upper lake under ice-covered conditions. Additionally, a clear reservoir effect is documented in Lake Fryxell and kinetic isotope effect associated with MSR as $\delta^{34}S_{SO4}$ and $\delta^{34}S_{H2S}$ show enrichments with depth of ~40‰ and ~30‰, respectively (Fig. 3; Saxton et al., 2016). The differences in sulfur isotopic behavior between these two ice-covered lake systems is likely related to the fact that Lake Fryxell is permanently ice-covered and amicitic versus the seasonally ice-covered, dimictic EVV Upper lake. The permanently stratified waters of Lake Fryxell allow for steep geochemical gradients and distinct microbial communities at different depths (e.g., Smith et al., 1993; Saxton et al., 2016) while EVV Upper lake undergoes seasonal stratification and mixing/overturn (Cadieux et al., 2017). Unfortunately, there are no $\delta^{34}S$ analyses of sedimentary sulfides from Lake Fryxell and therefore we cannot compare or evaluate the pyrite formation models for this ice-covered system.

6. Implications and conclusions

We have documented geochemical evidence for dynamic sulfur biogeochemical cycling that is tied to seasonal overturn and stratification periods within a small Arctic lake in western Greenland. Our analyses of surficial gossan deposits collected from nearby Upper EVV lake indicate a likely source of sulfate to this lake from nearby mafic dyke bedrock weathering which is directly underlying EVV Upper lake and/or a majority of its catchment in this part of the study area. Unlike other modern euxinic systems previously studied, EVV Upper lake undergoes seasonal ice-cover and is dimictic. Our $\delta^{34}S$ profiles during open-water euxinic conditions can be explained by both reservoir and kinetic isotope effects associated with MSR in stratified bottom waters that set up after ice-thaw and overturn in the spring. During ice-covered euxinic conditions, our water column $\delta^{34}S_{SO4}$ and $\delta^{34}S_{H2S}$ profiles exhibit larger fractionations ($\Delta^{34}S_{H2S}$) than open-water conditions, but no evidence of a reservoir effect. Additionally, sulfate concentrations and cell-specific sulfate reduction rates in EVV Upper lake appear to be the primary factors that influence the expression of the kinetic isotope effect associated with MSR. Our data supports previous studies that have indicated that in low-sulfate systems sulfate concentrations constrain ε_{SR} and its expression in $\delta^{34}S$ values over biological and environmental controls (Habicht et al., 2002; Gomes and Hurtgen, 2015). Sulfur isotope mass balance suggests that ice-covered water column pyrite formation can account for ~50% sedimentary sulfides in uppermost lake sediments recovered under these conditions, with the remainder of the sedimentary sulfides being formed under the previous stratified open-water conditions. However, only ~5% of the sedimentary sulfides in the uppermost anoxic sediments under open-waters can be accounted for by pyrite formed during previous ice-covered euxinic conditions, suggesting that lake overturn conditions in spring may have oxidized the majority of pyrite formed under ice-cover in EVV Upper lake.

The large observed offsets (11 to 15‰) between $\Delta^{34}S$ preserved in euxinic sediments and measured ε_{SR} values are consistent with previous studies of diffusion-limited, stratified low-sulfate systems (< 5 mM) where $\Delta^{34}S$ represents an integration of pyrite formed at different locations within the water column and/or sediment and during different seasons as well due to time averaging of $\delta^{34}S_{pyr}$ (Ivanov, 1978; Nakagawa et al., 2012; Gomes and Hurtgen, 2013). However, modern low-sulfate systems $\Delta^{34}S$ values ($\delta^{34}S_{SO4} - \delta^{34}S_{sed.\ sulfides}$) are still positively correlated with sulfate concentration and this is likely due to the reservoir effects significant influence on $\delta^{34}S$ values. Sulfate concentrations in EVV Upper lake are low (~330–600 μM), especially when compared to the modern ocean and most Phanerozoic seawater estimates, but are likely comparable to Proterozoic–Archean sulfate concentrations (Kah et al., 2004; Lyons and Gill, 2010; Crowe et al., 2014b). Our data when combined with the few other studies of low-sulfate systems provide important constraints on paleoceaonographic interpretations of surface water $\delta^{34}S_{SO4}$ preserved as carbonate-associated sulfate (CAS) or evaporites, and bottom water/sediment $\delta^{34}S_{H2S}$ preserved as $\delta^{34}S_{pyr}$, which is time averaged. A reservoir effect could be important process when interpreting $\Delta^{34}S$ trends in ancient low-sulfate oceans in addition to kinetic isotope effects associated with MSR (Gomes and Hurtgen, 2013). The combination of isotope effects discussed here could potentially explain spatial heterogeneity seen in late Cambrian $\delta^{34}S_{CAS}$ and $\Delta^{34}S$ records through the SPICE (e.g., Gill et al., 2011). As local redox conditions become more reducing this could have impacted nearby water column $\delta^{34}S_{SO4}$ values if a reservoir effect is operating under already low-sulfate oceans and sluggish circulation conditions, thus amplifying isotopic signatures of changes in global marine redox state based upon the presence/absence of locally stratified water mass.

While investigations of modern low-sulfate systems are critical for gaining potential insights into Earth's ancient oceans, it's important to note that these systems are sensitive to changes in environment, particularly those in polar regions (Mueller et al., 2009). As the Arctic continues to warm at amplified rates compared to global averages, sulfur dynamics within this lake and other Arctic lake systems are likely to change. For example, shifts in methane cycling have been recently documented from EVV Upper lake (as well as other lakes in our study area) that have been attributed to an anomalously warm summer season (Cadieux et al., 2017). The results presented here highlight the complexity and seasonality of sulfur biogeochemical cycling within modern euxinic systems, specifically in polar aquatic environments where annual temperature variations play a key role in duration of ice-cover and strength of thermal stratification in these lakes systems. More broadly, modern studies of low-sulfate systems help to calibrate interpretations of ancient $\Delta^{34}S$ records generated from marine sediments that provide important information about past sulfate concentrations or changes in biological and environmental factors that can affect sulfur isotopic fractionation.

Acknowledgements

Funding for this research was provided by a NASA-ASTEP grant (# NNX11AJ01G). Editor-in-chief Michael Böttcher and two anonymous reviewers are thanked for their constructive comments and reviews that greatly improved an earlier version of this manuscript. We thank Amy Goldman for field assistance, and Benjamin Underwood and Peter Sauer for technical assistance with isotope analyses at SIRF-Indiana University at Bloomington. For logistical support, we gratefully acknowledge Polar Field Services Inc., Kangerlussuaq International Science Support, along with Ruth Droppo for technical drafting assistance.

Appendix A. Supplementary data

Supplementary data to this article can be found online at https://doi.org/10.1016/j.chemgeo.2018.08.013.

References

Anderson, N.J., Stedmon, C.A., 2007. The effect of evapoconcentration on dissolved organic carbon concentration and quality in lakes of SW Greenland. Freshw. Biol. 52 (2), 280–289.

Anderson, N.J., Harriman, R., Ryves, D.B., Patrick, S.T., 2001. Dominant factors controlling variability in the ionic composition of West Greenland Lakes. Arct. Antarct. Alp. Res. 33 (4), 418–425.

Anderson, N.J., et al., 2008. Climate versus in-lake processes as controls on the development of community structure in a low-arctic lake (South-West greenland). Ecosystems 11 (2), 307–324.

Bekker, A., et al., 2004. Dating the rise of atmospheric oxygen. Nature 427 (6970), 117–120.

Berner, R.A., 1985. Sulfate reduction, organic-matter decomposition and pyrite formation. Philos. Trans. R. Soc. A Math. Phys. Eng. Sci. 315 (1531), 25–38.

Berner, R.A., 2004. The Phanerozoic Carbon Cycle: CO2 and O2. Oxford University Press, New York.

Blattler, C.L., et al., 2018. Two-billion-year-old evaporites capture Earth's great oxidation. Science 360 (6386), 320–323.

Bottrell, S.H., Newton, R.J., 2006. Reconstruction of changes in global sulfur cycling from marine sulfate isotopes. Earth Sci. Rev. 75 (1–4), 59–83.

Brennan, S.T., Lowenstein, T.K., Cendon, D.I., 2013. The major-ion composition of cenozoic seawater: the past 36 million years from fluid inclusions in marine halite. Am. J. Sci. 313 (8), 713–775.

Brüchert, V., Pratt, L.M., 1996. Contemporaneous early diagenetic formation of organic and inorganic sulfur in estuarine sediments from St Andrew Bay, Florida, USA. Geochim. Cosmochim. Acta 60 (13), 2325–2332.

Brüchert, V., Knoblauch, C., Jorgensen, B.B., 2001. Controls on stable sulfur isotope fractionation during bacterial sulfate reduction in Arctic sediments. Geochim. Cosmochim. Acta 65 (5), 763–776.

Cadieux, S.B., et al., 2016. Large fractionations of C and H isotopes related to methane oxidation in Arctic lakes. Geochim. Cosmochim. Acta 187, 141–155.

Cadieux, S.B., White, J.R., Pratt, L.M., 2017. Exceptional summer warming leads to contrasting outcomes for methane cycling in small Arctic lakes of Greenland. Biogeosciences 14 (3), 559–574.

Canfield, D.E., 1998. A new model for Proterozoic ocean chemistry. Nature 396 (6710), 450–453.

Canfield, D.E., 2001. Biogeochemistry of sulfur isotopes. In: Stable Isotope Geochemistry. 43. pp. 607–636.

Canfield, D.E., 2005. The early history of atmospheric oxygen: homage to Robert A. Garrels. Annu. Rev. Earth Planet. Sci. 33, 1–36.

Canfield, D.E., Thamdrup, B., 1994. The production of S-34-depleted sulfide during bacterial disproportionation of elemental sulfur. Science 266 (5193), 1973–1975.

Canfield, D.E., Raiswell, R., Bottrell, S., 1992. The reactivity of sedimentary iron minerals toward sulfide. Am. J. Sci. 292 (9), 659–683.

Canfield, D.E., Habicht, K.S., Thamdrup, B., 2000. The Archean sulfur cycle and the early history of atmospheric oxygen. Science 288 (5466), 658–661.

Canfield, D.E., Farquhar, J., Zerkle, A.L., 2010. High isotope fractionations during sulfate reduction in a low-sulfate euxinic ocean analog. Geology 38 (5), 415–418.

Chanton, J.P., Martens, C.S., Goldhaber, M.B., 1987. Biogeochemical cycling in an organic-rich coastal marine basin. 7. Sulfur mass balance, oxygen-uptake and sulfide retention. Geochim. Cosmochim. Acta 51 (5), 1187–1199.

Chanton, J.P., Martens, C.S., Paull, C.K., 1991. Control of pore-water chemistry at the base of the Florida escarpment by processes within the platform. Nature 349 (6306), 229–231.

Chanton, J.P., Martens, C.S., Paull, C.K., Coston, J.A., 1993. Sulfur isotope and porewater geochemistry of Florida escarpment seep sediments. Geochim. Cosmochim. Acta 57 (6), 1253–1266.

Colcord, D.E., et al., 2015. Assessment of branched GDGTs as temperature proxies in sedimentary records from several small lakes in southwestern Greenland. Org. Geochem. 82, 33–41.

Connelly, J.N., van Gool, J.A.M., Mengel, F.C., 2000. Temporal evolution of a deeply eroded orogen: the Nagssugtoqidian Orogen, West Greenland. Can. J. Earth Sci. 37 (8), 1121–1142.

Crowe, S.A., et al., 2014a. Deep-water anoxygenic photosythesis in a ferruginous chemocline. Geobiology 12 (4), 322–339.

Crowe, S.A., et al., 2014b. Sulfate was a trace constituent of Archean seawater. Science 346 (6210), 735–739.

Farquhar, J., Bao, H.M., Thiemens, M., 2000. Atmospheric influence of Earth's earliest sulfur cycle. Science 289, 756–758.

Farquhar, J., Savarino, J., Airieau, S., Thiemens, M.H., 2001. Observation of wavelength-sensitive mass-independent sulfur isotope effects during SO_2 photolysis: implications for the early atmosphere. J. Geophys. Res. Planets 106, 32829–32839.

Feng, D., Roberts, H.H., 2011. Geochemical characteristics of the barite deposits at cold seeps from the northern Gulf of Mexico continental slope. Earth Planet. Sci. Lett. 309 (1–2), 89–99.

Fike, D.A., Grotzinger, J.P., Pratt, L.M., Summons, R.E., 2006. Oxidation of the Ediacaran Ocean. Nature 444 (7120), 744–747.

Fike, D.A., Bradley, A.S., Rose, C.V., 2015. Rethinking the ancient sulfur cycle. Annu. Rev. Earth Planet. Sci. 43 (43), 593–622.

Finnegan, S., Fike, D.A., Jones, D., Fischer, W.W., 2012. A temperature-dependent positive feedback on the magnitude of carbon isotope excursions. Geosci. Can. 39, 122–131.

Fry, B., Gest, H., Hayes, J.M., 1988. S-34/S-32 fractionation in sulfur cycles catalyzed by anaerobic-bacteria. Appl. Environ. Microbiol. 54 (1), 250–256.

Fry, B., et al., 1991. Stable isotope studies of the carbon, nitrogen and sulfur cycles in the Black-Sea and the Cariaco Trench. Deep Sea Res. A Oceanography Research Papers 38, S1003–S1019.

Gilhooly, W.P., Reinhard, C.T., Lyons, T.W., 2016. A comprehensive sulfur and oxygen isotope study of sulfur cycling in a shallow, hyper-euxinic meromictic lake. Geochim. Cosmochim. Acta 189, 1–23.

Gill, B.C., Lyons, T.W., Saltzman, M.R., 2007. Parallel, high-resolution carbon and sulfur isotope records of the evolving Paleozoic marine sulfur reservoir. Palaeogeogr. Palaeoclimatol. Palaeoecol. 256 (3–4), 156–173.

Gill, B.C., et al., 2011. Geochemical evidence for widespread euxinia in the later Cambrian ocean. Nature 469 (7328), 80–83.

Goldhaber, M.B., Kaplan, I.R., 1980. Mechanisms of sulfur incorporation and isotope fractionation during early diagenesis in sediments of the Gulf of California. Mar. Chem. 9 (2), 95–143.

Goldman, A.E., Cadieux, S.B., White, J.R., Pratt, L.M., 2016. Passive sampling method for high-resolution concentration and isotopic composition of dissolved methane in Arctic lakes. Limnol. Oceanogr. Methods 14 (2), 69–78.

Gomes, M.L., Hurtgen, M.T., 2013. Sulfur isotope systematics of a euxinic, low-sulfate lake: evaluating the importance of the reservoir effect in modern and ancient oceans. Geology 41 (6), 663–666.

Gomes, M.L., Hurtgen, M.T., 2015. Sulfur isotope fractionation in modern euxinic systems: Implications for paleoenvironmental reconstructions of paired sulfate-sulfide isotope records. Geochim. Cosmochim. Acta 157, 39–55.

van Gool, J.A.M., Kriegsman, L.M., Marker, M., Nichols, G.T., 1999. Thrust stacking in the inner Nordre Stromfjord area, West Greenland - significance for the tectonic evolution of the Palaeoproterozoic Nagssugtoqidian orogen. Precambrian Res. 93 (1), 71–86.

van Gool, J.A.M., et al., 2002a. Precambrian geology of the northern Nagssugtoqidian orogen, West Greenland: mapping in the Kangaatsiaq area. Geol. Greenl. Surv. Bull. 191, 13–23.

van Gool, J.A.M., Connelly, J.N., Marker, M., Mengel, F.C., 2002b. The Nagssugtoqidian Orogen of West Greenland: tectonic evolution and regional correlations from a West Greenland perspective. Can. J. Earth Sci. 39 (5), 665–686.

Guo, Q.J., et al., 2009. Reconstructing Earth's surface oxidation across the Archean-Proterozoic transition. Geology 37 (5), 399–402.

Habicht, K.S., Canfield, D.E., 1996. Sulphur isotope fractionation in modern microbial mats and the evolution of the sulphur cycle. Nature 382 (6589), 342–343.

Habicht, K.S., Canfield, D.E., Rethmeier, J., 1998. Sulfur isotope fractionation during bacterial reduction and disproportionation of thiosulfate and sulfite. Geochim. Cosmochim. Acta 62 (15), 2585–2595.

Habicht, K.S., Gade, M., Thamdrup, B., Berg, P., Canfield, D.E., 2002. Calibration of sulfate levels in the Archean Ocean. Science 298 (5602), 2372–2374.

Halevy, I., Peters, S.E., Fischer, W.W., 2012. Sulfate burial constraints on the phanerozoic sulfur cycle. Science 337 (6092), 331–334.

Harrison, A.G., Thode, H.G., 1958. Mechanism of the bacterial reduction of sulphate from isotope fractionation studies. Trans. Faraday Soc. 54 (1), 84–92.

Hartmann, M., Nielsen, H., 1969. δ34S-Werte in rezenten Meeressedimenten und ihre Deutung am Beispiel einiger Sedimentprofile aus der westlichen Ostsee. Geol. Rundsch. 58, 621.

Hartmann, M., Nielsen, H., 2012. delta S-34 values in recent sea sediments and their significance using several sediment profiles from the western Baltic Sea. Isot. Environ. Health Stud. 48 (1), 7–32.

Henriksen, N., Higgins, A.K., Kalsbeek, F., Pulvertaft, T.C.R., 2009. Greenland from Archean to Quaternary: descriptive text to the 1995 geologic map of Greenland, 1:2 500 000. In: Garde, A.E. (Ed.), Geological Survey of Denmark and Greenland Bulletin. Geological Survey of Denmark and Greenland, Copenhagen, Denmark, pp. 14–32.

Holland, H.D., 2006. The oxygenation of the atmosphere and oceans. Philos. Trans. R. Soc. B 361 (1470), 903–915.

Horita, J., Zimmermann, H., Holland, H.D., 2002. Chemical evolution of seawater during the Phanerozoic: implications from the record of marine evaporites. Geochim. Cosmochim. Acta 66 (21), 3733–3756.

Hurtgen, M.T., Arthur, M.A., Suits, N.S., Kaufman, A.J., 2002. The sulfur isotopic composition of Neoproterozoic seawater sulfate: implications for a snowball Earth? Earth Planet. Sci. Lett. 203 (1), 413–429.

Hurtgen, M.T., Halverson, G.P., Arthur, M.A., Hoffman, P.F., 2006. Sulfur cycling in the aftermath of a 635-Ma snowball glaciation: evidence for a syn-glacial sulfidic deep ocean. Earth Planet. Sci. Lett. 245 (3–4), 551–570.

Ivanov, M.V., 1978. Influence of microorganisms and microenvironment on the global sulfur cycle. In: Environmental Biogeochemistry and Geomicrobiology, Ann Arbor, Michigan, pp. 47–61.

Jensen, S.M., et al., 2002. Kimberlites and other ultramafic alkaline rocks in the Sisimiut-Kangerlussuaq region, southern West Greenland. Geol. Greenl. Surv. Bull. 191, 57–66.

Johnston, D.T., 2010. Touring the Biogeochemical Landscape of a Sulfur-Fueled World. Elements 6 (2), 101–106.

Johnston, D.T., 2011. Multiple sulfur isotopes and the evolution of Earth's surface sulfur cycle. Earth Sci. Rev. 106 (1–2), 161–183.

Jørgensen, B.B., 1982. Mineralization of Organic-Matter in the Sea Bed - the Role of Sulfate Reduction. Nature 296 (5858), 643–645.

Jørgensen, A.S., Andreasen, F., 2007. Mapping of permafrost surface using ground-penetrating radar at Kangerlussuaq Airport, western Greenland. Cold Reg. Sci. Technol. 48 (1), 64–72.

Kah, L.C., Lyons, T.W., Frank, T.D., 2004. Low marine sulphate and protracted oxygenation of the proterozoic biosphere. Nature 431 (7010), 834–838.

Kaplan, I.R., Rittenberg, S.C., 1964. Microbiological fractionation of sulphur isotopes. J. Gen. Microbiol. 34 (2), 195–212.

Kemp, A.L.W., Thode, H.G., 1968. Mechanism of bacterial reduction of sulphate and of sulphite from isotope fractionation studies. Geochim. Cosmochim. Acta 32 (1), 71 (&).
Larsen, L.M., Rex, D.C., 1992. A review of the 2500-Ma span of alkaline-ultramafic, potassic and carbonatitic magmatism in West Greenland. Lithos 28 (3–6), 367–402.
Leavitt, W.D., Halevy, I., Bradley, A.S., Johnston, D.T., 2013. Influence of sulfate reduction rates on the Phanerozoic sulfur isotope record. Proc. Natl. Acad. Sci. U. S. A. 110 (28), 11244–11249.
Lefticariu, L., Pratt, L.M., Ripley, E.M., 2006. Mineralogic and sulfur isotopic effects accompanying oxidation of pyrite in millimolar solutions of hydrogen peroxide at temperatures from 4 to 150 degrees C. Geochim. Cosmochim. Acta 70 (19), 4889–4905.
Lowenstein, T.K., Hardie, L.A., Timofeeff, M.N., Demicco, R.V., 2003. Secular variation in seawater chemistry and the origin of calcium chloride basinal brines. Geology 31 (10), 857–860.
Lowenstein, T.K., Timofeeff, M.N., Kovalevych, V.M., Horita, J., 2005. The major-ion composition of Permian seawater. Geochim. Cosmochim. Acta 69 (7), 1701–1719.
Lyons, T.W., 1997. Sulfur isotopic trends and pathways of iron sulfide formation in upper Holocene sediments of the anoxic Black Sea. Geochim. Cosmochim. Acta 61 (16), 3367–3382.
Lyons, T.W., Gill, B.C., 2010. Ancient sulfur cycling and oxygenation of the early biosphere. Elements 6 (2), 93–99.
Lyons, T.W., Werne, J.P., Hollander, D.J., Murray, R.W., 2003. Contrasting sulfur geochemistry and Fe/Al and Mo/Al ratios across the last oxic-to-anoxic transition in the Cariaco Basin, Venezuela. Chem. Geol. 195 (1–4), 131–157.
Lyons, T.W., Walter, L.M., Gellatly, A.M., Martini, A.M., Blake, R.E., 2004. Sites of anomolous organic remineralization in the carbonate sediments of South Florida, USA: The sulfur cycle and carbonate-associated sulfate. In: Amend, J.P., Edwards, K.J., Lyons, T.W. (Eds.), Sulfur Biogeochemistry Past and Present. Geological Society of America Special Paper Vol. 379. pp. 161–178.
Mariotti, A., et al., 1981. Experimental-determination of nitrogen kinetic isotope fractionation - some principles - illustration for the denitrification and nitrification processes. Plant Soil 62 (3), 413–430.
Mueller, D.R., Van Hove, P., Antoniades, D., Jeffries, M.O., Vincent, W.F., 2009. High Arctic lakes as sentinel ecosystems: cascading regime shifts in climate, ice cover, and mixing. Limnol. Oceanogr. 54 (6), 2371–2385.
Nakagawa, M., et al., 2012. Seasonal change in microbial sulfur cycling in monomictic Lake Fukami-ike, Japan. Limnol. Oceanogr. 57 (4), 974–988.
Nutman, A.P., Kalsbeek, F., Marker, M., van Gool, J.A.M., Bridgwater, D., 1999. U-Pb zircon ages of Kangamiut dykes and detrital zircons in metasediments in the Palaeoproterozoic Nagssugtoqidian Orogen (West Greenland) - Clues to the pre-collisional history of the orogen. Precambrian Res. 93 (1), 87–104.
Nutman, A.P., Kalsbeek, F., Friend, C.R.L., 2008. The Nagssugtoqidian orogen in South-East Greenland: evidence for Paleoproterozoic collision and plate assembly. Am. J. Sci. 308 (4), 529–572.
Overmann, J., Tilzer, M.M., 1989. Control of primary productivity and the significance of photosynthetic bacteria in a Meromictic Kettle Lake - Mittlerer-Buchensee, West-Germany. Aquat. Sci. 51 (4), 261–278.
Overmann, J., Beatty, J.T., Hall, K.J., Pfennig, N., Northcote, T.G., 1991. Characterization of a dense, purple sulfur bacterial layer in a Meromictic Salt Lake. Limnol. Oceanogr. 36 (5), 846–859.
Pavlov, A.A., Hurtgen, M.T., Kasting, J.F., Arthur, M.A., 2003. Methane-rich Proterozoic atmosphere? Geology 31 (1), 87–90.
Postgate, J.R., 1984. The Sulphate-reducing Bacteria. Cambridge University Press, Cambridge (122 pp).
Poulton, S.W., Fralick, P.W., Canfield, D.E., 2010. Spatial variability in oceanic redox structure 1.8 billion years ago. Nat. Geosci. 3 (7), 486–490.
Raiswell, R., Canfield, D.E., 2012. The iron biogeochemical cycle past and present. Geochem. Perspect. 1 (1), 1–220.
Reeburgh, W.S., 2007. Oceanic methane biogeochemistry. Chem. Rev. 107 (2), 486–513.
Rees, C.E., Jenkins, W.J., Monster, J., 1978. Sulfur isotopic composition of ocean water sulfate. Geochim. Cosmochim. Acta 42 (4), 377–381.
Rudnicki, M.D., Elderfield, H., Spiro, B., 2001. Fractionation of sulfur isotopes during bacterial sulfate reduction in deep ocean sediments at elevated temperatures. Geochim. Cosmochim. Acta 65 (5), 777–789.
Saxton, M.A., et al., 2016. Biogeochemical and 16S rRNA gene sequence evidence supports a novel mode of anaerobic methanotrophy in permanently ice-covered Lake Fryxell, Antarctica. Limnol. Oceanogr. 61, S119–S130.
Sim, M.S., Bosak, T., Ono, S., 2011a. Large sulfur isotope fractionation does not require disproportionation. Science 333 (6038), 74–77.
Sim, M.S., Ono, S., Donovan, K., Templer, S.P., Bosak, T., 2011b. Effect of electron donors on the fractionation of sulfur isotopes by a marine Desulfovibrio sp. Geochim. Cosmochim. Acta 75 (15), 4244–4259.
Sim, M.S., Ono, S., Bosak, T., 2012. Effects of iron and nitrogen limitation on sulfur isotope fractionation during microbial sulfate reduction. Appl. Environ. Microbiol. 78 (23), 8368–8376.
Smith, R.L., Miller, L.G., Howes, B.L., 1993. The geochemistry of methane in Lake Fryxell, an Amictic, permanently ice-covered, Antarctic Lake. Biogeochemistry 21 (2), 95–115.
Spear, N., et al., 2014. Analyses of fluid inclusions in Neoproterozoic marine halite provide oldest measurement of seawater chemistry. Geology 42 (2), 103–106.
Stanley, S.M., 2010. Relation of Phanerozoic stable isotope excursions to climate, bacterial metabolism, and major extinctions. Proc. Natl. Acad. Sci. U. S. A. 107 (45), 19185–19189.
Szynkiewicz, A., Moore, C.H., Glamoclija, M., Pratt, L.M., 2009. Sulfur isotope signatures in gypsiferous sediments of the Estancia and Tularosa Basins as indicators of sulfate sources, hydrological processes, and microbial activity. Geochim. Cosmochim. Acta 73 (20), 6162–6186.
Thompson, R.L., et al., 2017. Methane fluxes in the high northern latitudes for 2005–2013 estimated using a Bayesian atmospheric inversion. Atmos. Chem. Phys. 17 (5), 3553–3572.
Turchyn, A.V., Sivan, O., Schrag, D.P., 2006. Oxygen isotopic composition of sulfate in deep sea pore fluid: evidence for rapid sulfur cycling. Geobiology 4 (3), 191–201.
Weber, H.S., Thamdrup, B., Habicht, K.S., 2016. High sulfur isotope fractionation associated with anaerobic oxidation of methane in a low-sulfate, iron-rich environment. Front. Earth Sci. 4.
Wortmann, U.G., Paytan, A., 2012. Rapid variability of seawater chemistry over the past 130 million years. Science 337 (6092), 334–336.
Wortmann, U.G., Bernasconi, S.M., Bottcher, M.E., 2001. Hypersulfidic deep biosphere indicates extreme sulfur isotope fractionation during single-step microbial sulfate reduction. Geology 29 (7), 647–650.
Young, S.A., Loukola-Ruskeeniemi, K., Pratt, L.M., 2013. Reactions of hydrothermal solutions with organic matter in Paleoproterozoic black shales at Talvivaara, Finland: evidence from multiple sulfur isotopes. Earth Planet. Sci. Lett. 367, 1–14.
Zerkle, A.L., Farquhar, J., Johnston, D.T., Cox, R.P., Canfield, D.E., 2009. Fractionation of multiple sulfur isotopes during phototrophic oxidation of sulfide and elemental sulfur by a green sulfur bacterium. Geochim. Cosmochim. Acta 73 (2), 291–306.